Chapter 3

Cartilage ultrastructure in proteoglycan-deficient zebrafish mutants brings to light new candidate genes for human skeletal disorders

Malgorzata I Wiweger, Cristina M Avramut,
Carlos E de Andrea, Frans A Prins,
Abraham J Koster, Raimond BG Ravelli,
Pancras CW Hogendoorn
Journal of Pathology 2011;223: 531-42

Abstract

Proteoglycans are molecules consisting of protein cores onto which sugar chains, i.e., glycosaminoglycans (GAGs) such as heparan or chondroitin sulphates, are attached. Proteoglycans are produced by nearly all cells, and once secreted they become a major component of the extracellular matrix. Cartilage is particularly rich in proteoglycans, and changes in the structure and composition of GAGs have been found in osteochondromas and osteoarthritis. The zebrafish (*Danio rerio*) exhibits fast development, a growth plate-like organization of its craniofacial skeleton and an availability of various mutants, making it a powerful model for the study of human skeletal disorders with unknown aetiology. We analysed skeletons from five zebrafish lines with known mutations in genes involved in proteoglycan synthesis: *dackel* (*dak/ext2*), lacking heparan sulphate; *hi307* (β*3gat3*), deficient for most GAGs; *pinscher* (*pic/slc35b2*), presenting defective sulphation of GAGs and other molecules; *hi954* (*uxs1*), lacking Notch and most GAGs due to impaired protein xylosylation; and *knypek* (*kny/gpc4*), missing the protein core of the Glypican-4 proteoglycan. Here we show that each mutant displays different phenotypes related to: (a) cartilage morphology; (b) composition of the extracellular matrix; (c) ultrastructure of the extracellular matrix; and (d) the intracellular ultrastructure of chondrocytes, proving that sulphated GAGs orchestrate the cartilage intra- and extracellular ultrastructures. The mild phenotype of the *hi307* mutant suggests that proteoglycans consisting of a protein core and a short sugar linker might suffice for proper chondrocyte stacking. Finally, *knypek* supports the involvement of Glypican-4 in the craniofacial phenotype of Simpson–Golabi–Behmel syndrome and suggests GPC4 as a modulator of the overgrowth phenotype that is associated with this syndrome and is primarily caused by a mutation in *GPC3*. Moreover, we speculate on the potential involvement of *SLC35B2*, β*3GAT3* and *UXS1* in skeletal dysplasias. This work promotes the use of zebrafish as a model of human skeletal development and associated pathologies.

Keywords: bone; cartilage; electron microscopy; glycans; osteochondroma; skeletal dysplasia; zebrafish

Introduction

The development, growth and functionality of living organisms require the presence of poly- and oligosaccharides known as glycans. Unbranched polysaccharides such as heparan sulphate (HS), chondroitin sulphate (CS), dermatan sulphate (DS) and keratan sulphate (KS) constitute a group of glycosaminoglycans (GAGs) and, when attached to a protein, form proteoglycans. GAGs/proteoglycans are produced by nearly all types of cells, but they are especially abundant in the cartilage extracellular matrix, where, together with other components of the extracellular matrix, they control many cellular events, such as adhesion, migration and differentiation [1]. This regulatory function is attributed to the various binding properties of GAGs. GAGs not only bind proteins but, also retain water molecules, thereby maintaining cartilage elasticity. Hence, it is not surprising that changes in GAG/proteoglycan structure and composition have physiological and pathological implications. For example, mutations in *EXT1* or *EXT2*, two genes that are crucial for the biosynthesis of HS, cause the development of osteochondroma, a benign cartilage-capped bone tumour [2]. Mutations in other HS-related genes have also been linked to skeletal conditions; e.g. mutation in *PERLECAN* leads to dyssegmental dysplasia [3], disruption of *GLYPICAN 3* causes Simpson–Golabi–Behmel syndrome [4], mutation in *GLYPICAN 6* results in recessive omodysplasia [5], and CS deficiency related to a mutation in the *CHST3* gene is found in spondylo-epi(meta) physeal dysplasia Omani type 6, 7. Mutations in the genes involved in the sulphation of proteoglycans are also known to cause several dysplasias (for a review, see Superti-Furga and Unger, 2007).

Different approaches and models are available for studies on diseases/disorders caused by GAG/proteoglycan dysfunction. Zebrafish (*Danio rerio*) is a popular model due to its fast development, the transparency of its embryos, its ease of manipulation at the molecular level and the availability of various mutants. The simple organization of the zebrafish skeleton and a similar developmental pattern to that of mammals makes zebrafish particularly useful for studies on skeletal development and disease. The craniofacial cartilage is one of the first to be formed during fish development. The first elements develop as early as 2 days post-fertilization (dpf) to give a fully functional cartilaginous skeleton by 5 dpf [8].

To learn more about the function of different glycans in human skeletal development and disease, we characterized the cartilage of wild-type (AB) zebrafish and five homozygous mutant lines with different defects in glycan synthesis. The mutants used in this study were identified by different groups: *dackel* (*dak/ext2*) and *pinscher* (*pic/slc35b2*, previously named *papst1*) [9], as well as *hi307* (β*3gat3*) and *hi954* (*uxs1*) [10] were selected based on their cartilage phenotypes, while *knypek* (*kny/gpc4*) was first recognized as a mutant with defective gastrulation movements [11]. Based on the functions of *ext2*, *gpc4*, *slc35b2*, β*3gat3* and *uxs1*, the biosynthesis of GAGs/proteoglycans should be affected at different steps: *dak* should lack HS only, *kny* should lack only a small population of HS, pic

should have reduced levels of sulphated CS, DS, HS, KS and non-GAG molecules, *hi307* should be deficient in CS, DS and HS, and *hi954* (*uxs1*) should lacks CS, DS, HS and other molecules requiring xylosylation (Table 1). Using light microscopy and transmission electron microscopy, we characterised the skeletons of proteoglycans-deficient zebrafish mutants and addressed the functions of different glycans in cartilage development, allowing us to speculate on the potential homology with human skeletal dysplasias.

Materials and methods

Animals

Zebrafish (*Danìo rerio H.*) embryos were obtained in natural crosses and staged in accordance with Kimmel et al [12]. Wild-type (AB) and five null mutants {*dackel* (*dak*), *exostoses (multiple) 2 allele ext2A*^{0739}; *pinscher* (*pic*), *solute carrier family 35*, *member B2 allele slc35b2*^{14MX} (previously named *PAPS transporter 1*, *papst1*) [9]; hi307, *ß1,3-glucuronyltransferase 3 allele* β*3gat3*^{hi307} [10]; *hi954*, *UDP–glucuronic acid decarboxylase 1 allele uxs1hi95410; and knypek (kny), and glypican 4 allele gpc4*^{V348} [11]} were raised to 5 dpf. Prior to fixation or freezing (GAG assay), the fish were anaesthetized in Tricane, and homozygous mutants were sorted by phenotype.

Human cartilage

Postnatal growth plates and osteochondromas were sampled at the Leiden University Medical Centre. Growth plates were from orthopaedic resections for pathological conditions not related to osteochondroma. All samples were obtained and handled according to ethical guidelines as described in the *Code for Proper Secondary Use of Human Tissue in The Netherlands* of the Dutch Federation of Medical Scientific Societies.

GAG assay

At 5 dpf, homozygous mutants were sorted by phenotype, and pools of 10 WT and sorted homozygote mutants were frozen for at least 1 h at − 20 °C prior to GAG extraction. GAG extraction and quantification was performed according to the Blyscan sulphated glycan assay manual (Biocolor, UK). GAG assays were performed three times in duplicate.

Light microscopy and immunohistology

Unless stated otherwise, all experimental procedures were performed as described previously 13. Fish were embedded in paraffin and cut into 4 µm sections. For glycogen detection only, after deparaffinization and rehydration, samples were incubated for 30 min at 60 °C in periodic acid, rinsed in water and stained with Schiff reagent for 30 min at room temperature. After a 15 min wash in water, the slides were dehydrated, mounted in micromount (Surgipath) and analysed under a light microscope.

Table 1. Theoretical changes in the biosynthesis of biologically active molecules predicted based on the known functions of the *exostosin 2* (*ext2*), *Glypican 4* (*gpc4*), *solute carrier family 35*, *member B2* (*slc35b2*); β*1,3-glucuronyltransferase 3* (β*3gat3*) and *UDP-glucuronic acid decarboxylase 1* (*uxs1*) genes.

Gene Mutant	*ext2 dackel*	*gpc4 knypek*	*slc 35b2 pinscher*	*b3gat3 hi307*	*uxs1 hi954*
Chondroitin sulphate	na	na	Reduction	Loss	Loss
Dermatan sulphate	na	na	Reduction	Loss	Loss
Heparan sulphate	Loss	Reduction	Reduction	Loss	Loss
Hyaluronan	na	na	na	na	na
Keratan sulphate	na	na	Reduction	na	na
Other molecules	na	na	Loss of all sulphated molecules	na	Loss of Notch, blood coagulation factor VII and IX

Loss, full inhibition of biosynthesis; reduction, only some molecules are affected, eg the loss of sulphated epitopes in the pic mutant; na, not affected.

Sections predigested for 30 min at 37 °C in α-amylase (0.5% w/v in PBS; Sigma) were included as negative controls. For immunostaining of the extracellular matrix, anti-CS (CS-56, Sigma) at 1:800, anti-collagen type II (II-II6B3, Developmental Studies Hybridoma Bank) at 1:200, anti-collagen I (Rockland) at 1:800 and anti-collagen VI at 1:50 (Abcam) were used as primary antibodies. The poly-HRP-Gam/R/R IgG system (ImmunoLogic), followed by DAB detection (Dako) or anti-mouse AP (Sigma) at 1:500, followed by BCIP/NBT (Sigma), was used to detect the signal. Each experiment was repeated at least three times with the same results.

Transmission electron microscopy

Fish were fixed in either: (a) 1.5% glutaraldehyde; (b) a mixture of 1.5% glutaraldehyde and 1% PFA; or (c) a mixture of 1.5% glutaraldehyde and 4% PFA; all were in 0.1 m sodium cacodylate for 1 h, followed by incubation in 1% osmium tetroxide (OsO4) in 0.1 m sodium cacodylate for 1 h. After each step of the fixation, the fish were rinsed twice with 0.1 m sodium cacodylate and finally dehydrated in a series of 70%, 80%, 90% and 3× 100% ethanol, prior to immersion in a 1:1 epon:propylene oxide solution for 1 h. The samples were washed afterwards with pure epon, embedded in pure epon LX112 and polymerized at 60 °C for 2 days. Cross-sections (800 nm thick) from five homozygous mutant fish from each line were stained with toluidine blue and analysed for general morphological figures under a light microscope. The pilot experiment revealed that WT fish fixed in 1.5% glutaraldehyde with and without addition of PFA had similar morphologies, and for further analysis all fish were fixed in 1.5% glutaraldehyde, omitting the PFA. The cartilage ultrastructures were analysed by transmission electron microscopy in the WT and two homozygous mutants from each line. For this purpose, transverse sections of 100 nm thickness were transferred to slot grids for transmission electron microscopy and post-stained with 7% uranyl acetate and Reynolds' lead citrate. The percentage of the extracellular matrix space that was filled with fibres was analysed on the electron micrographs.

Results

Concentration of total sulphated GAGs

Although the Blyscan assay does not give any indication of the concentration of single CS, KS, DS or HS, it allows for the quantification of the total level of sulphated GAGs (free and as a part of proteoglycans) present in a sample. Compared to WT, significantly decreased levels of total sulphated GAGs were detected in *pic*, *hi307* and *hi954* homozygous mutants (Figure 1), which was in line with the theoretical predictions based on what is known about the functions of *slc35b2*, β*3gat3* and *uxs1*, respectively (Table 1). A normal level of total sulphated GAGs was detected in the *kny* mutant, which lacks Glypican 4 (Figure 1). Intriguingly, the level of total sulphated GAGs in the dak mutant was elevated (Figure 1), even though a mutation in *ext2* should inhibit HS synthesis (Table 1).

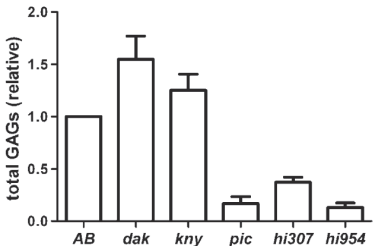

Figure 1. Relative levels of total sulphated GAGs at 5 dpf in WT and homozygote mutants: *dackel* (*dak/ext2*), *knypek* (*kny/gpc4*), *pinscher* (*pic/slc35b2*), *hi307* (β*3gat3*) and *hi954* (*uxs1*). The level of sulphated GAGs in *kny* is similar to that in WT. The *dak* mutant has a significantly higher content of sulphated GAGs than WT, whereas *pic*, *hi307* and *hi954* contain significantly lower levels of sulphated GAGs than WT.

Cartilage morphology

At 5 dpf, wild-type chondrocytes in pharyngeal arches were organized into neat stacks of cells flattened along the longitudinal axis, thus resembling chondrocytes from the proliferating zone of the mammalian growth plate (Figure 2C',D). From the analysed mutants, the morphologies of *hi307* (which in theory should lack most of proteoglycans) and *kny* (which should lack Glypican 4 only) were the most similar to WT. Although the chondrocytes in Meckel's and ceratohyal cartilages did not stack well (Figure 3A), *hi307*- and *kny*-derived chondrocytes were properly stacked and flattened in other craniofacial cartilage elements (Figure 3B). *dak*, which should lack HS only, and *pic*, which has impaired sulphation, had very severe cartilage phenotypes (Figure 3A, B). In both mutants, all chondrocytes were similar to those from human OCs, ie they were rounded and did not intercalate into stacks but remained as a disorganized cluster of cells (Figures 2E, 3A, B). In the *hi954* mutant, which should lack most GAGs and other xylated molecules, chondrocytes had an atypical appearance, often failed to intercalate and were deficient in the extracellular matrix (Figures 3B, 5B).

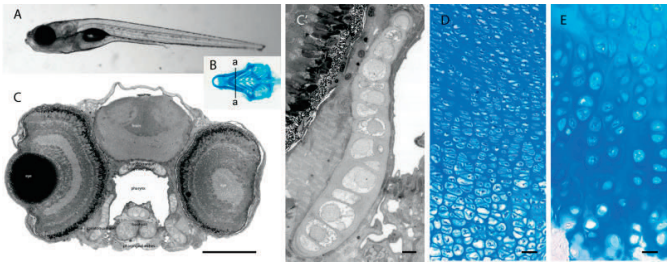

Figure 2. The organization of the cartilaginous skeleton in zebrafish at 5 dpf. WT chondrocytes in pharyngeal arches are organized into neat stacks of chondrocytes flattened along the longitudinal axis, thus resembling chondrocytes from the proliferating zone of the mammalian growth plate. Lateral view of 4 mm zebrafish WT larvae (A); craniofacial skeleton visualized by whole-mount staining with alcian blue (B); transverse section at the level indicated by aa (C); magnification of the area with palatoquadrate (C'); growth plate from a human fetus (D); cartilage cap from an osteochondroma (E). Scale bar = 5 µm (C) and 100 µm (D, E)

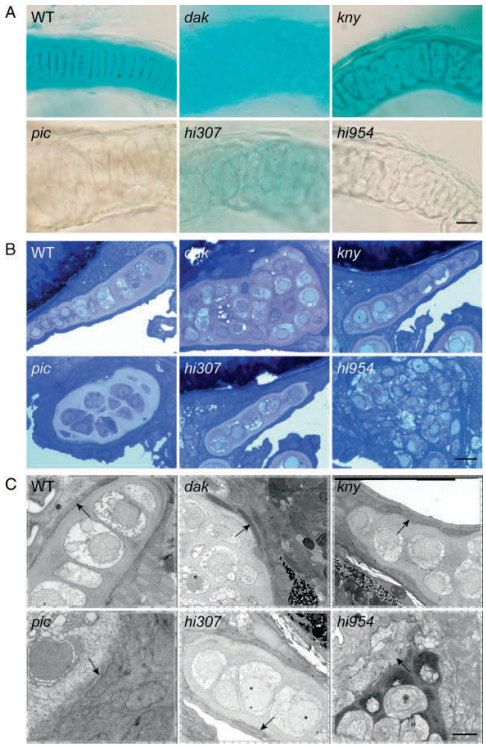

Figure 3. Defects in cartilage organization and extracellular matrix composition in proteoglycan-deficient homozygote mutants: *dackel* (*dak/ext2*), *knypek* (*kny/gpc4*), *pinscher* (*pic/slc35b2*), *hi307* (*β3gat3*) and *hi954* (*uxs1*). Neat stacks of chondrocytes flattened along the longitudinal axis are present in WT (A, B). In *kny* and *hi307*, mild chondrocyte clustering can be observed only in Meckel's and ceratohyal cartilages (A), whereas other cartilage elements appear normal (B). A loss of stacking similar to that in human OCs is especially apparent in the dak and pic mutants (A, B). *hi954* chondrocytes have an atypical appearance, with severely reduced extracellular matrix and often failure to intercalate (A). The lack of blue staining (A) and purple staining (B) in cartilage from *pic*, *hi307* and *hi954* mutants confirms the absence of sulphated proteoglycan in the extracellular matrix. The severely reduced extracellular matrix in the *hi954* mutant should be noted. Normally, cartilage elements are surrounded with a perichondrium made up of one to two layers of small, elongated cells, with little cytoplasm and extracellular matrix but rich in electron-dense material. *dak*, *kny* and *hi307* show normal perichondrium; the pic perichondrium is thicker; no perichondrium can be identified in *hi954*. The whole-mount Meckels' cartilage was stained by alcian blue (A). Sections at the level of the palatoquadrate were stained with toluidine blue (B). The perichondriums in WT and homozygous mutant fish are shown at 5 dpf (C). Scale bar = 5 µm (A), 10 µm (B) and 5 µm (C)

The spacing between WT fish chondrocytes was less pronounced than in human cartilage, but it was similarly filled with a glycan-rich extracellular matrix (Figures 2C',3). The *hi954* mutant was the only mutant that showed a severely reduced extracellular matrix deposition. None of the other mutants showed any sign of reductions or increases in the extracellular matrix accumulation (Figure 3B). In contrast to what is known from higher vertebrates, numerous lacunae enclosing small groups of chondrocytes are not present in zebrafish. However, lacunae-like borders were observed at the periphery of each cartilage element (Figure 3B, C). Therefore, we concentrated on the areas between chondrocytes where the extracellular matrix was homogeneous and looked like typical immature hyaline cartilage.

Perichondrium

In WT fish, chondrocyte elements were surrounded with a thin layer of perichondrium made up of one or two layers of small, elongated cells, with little cytoplasm and extracellular matrix but rich in electron-dense material (Figure 3C). Similar perichondria were also observed in *dak*, *kny* and *hi307* mutants (Figure 3C). The *pic* perichondrium was thickened, showing enlarged cells and a rough surface (Figure 3C). In the case of *hi954*, typical perichon-drium-like cells were not present; however, chondrocytes were neighboured by slightly elongated cells that had variable sizes, rough surfaces and were rich in cytoplasm but were poor in electron-dense material (Figure 3C).

Bone ossification

As cartilage prefigures the development of cartilage bones in fish (analogous to endochondral bones in mammals), we were interested to determine whether bone development was affected in our mutants. By 5 dpf, most of the bones stained by alizarin red were of intramembranous origin (i.e. bones that do not form upon a cartilage template; see supporting information, Table S1). Of those, the cleithrum and opercle, the first bones to develop, were found in WT and all mutant fish; however, in *dak*, *pic* and *hi307* mutants they were small and malformed (data not shown). Other dermal bones were unaffected in *kny*, *hi307* and *hi954* but were severely reduced/lost in *dak* and *pic* mutants (see supporting information, Table S1). When it comes to the cartilage bones (fish) that correspond to endochondral bones in mammals, by 5 dpf WT ossification was seen only in the 5th ceratobranchial. No alterations in bone development, including bone malformations and changes in the timing of ossification, were observed in the *kny*, *hi307* and *hi954* mutants. However, at later time-points, delays in the development of other cartilage bones were observed in *hi307* and *hi954* mutants (data not shown). The 5th arch from dak ossified normally despite severe malformations of its cartilaginous template, whereas pic ossification was reduced (see supporting information, Table S1). The blockage of cartilage bone formation in dak and pic mutants was more severe than in *hi* mutants and it persisted until at least 9 dpf (data not shown).

Secretion and composition of the extracellular matrix

The zebrafish extracellular matrix, like any other cartilage matrix from vertebrates, consists mostly of water, collagens and proteoglycans. In WT cartilage, proteoglycans stain blue with alcian blue (Figure 3A) and purple with toluidine blue (Figure 3B). Cartilage from WT, *dak* and *kny* were stained with both dyes. *hi954* remained unstained (Figure 3A, B), whereas the skeletons of *pic* and *hi307* showed pale staining (Figure 3A, B). Those observations are in line with previous reports on alcian blue stains in *dak* and *pic* [13], *hi307* [14] and *hi954* [14, 15] and also correlate well with the results from the GAG assay (Figure 1). We also examined the deposition of Collagen II and found that this protein was absent in the *hi954* mutant and significantly reduced in *hi307*, whereas other mutants did not show any abnormalities in the production of this extracellular matrix component (Figure 4B, Table 2). Collagen I and VI were normally expressed in *dak* and *kny* mutants but were reduced/absent in the *hi307* and *hi954* mutants (Figure 4B, Table 2).

Ultrastructure of the extracellular matrix

The collagen network, consisting of a net of long and thin collagen fibres associated with proteoglycan granules (electron-dense particles), was clearly visible in the extracellular matrix of WT chondrocytes (Figure 4A). The fibrils present between well-stacked chondrocytes were mostly orientated perpendicular to the longitudinal axis of cartilage elements (aligned fibres), whereas presumptively intercalating chondro-cytes were surrounded with a radially running collagen network (radial fibres) (see supporting information, Figure S1). In WT, aligned fibres were observed in 47% and radial fibres in 37% of extracellular spaces. No apparent fibrils were observed in the remaining 16% of cases. A WT-like collagen network and proteoglycan granules were also observed in the *kny* mutant (Figure 4A). *kny* had aligned and radial fibres observed in 24% and 52% of extracellular spaces, respectively. In the *dak* mutant, collagen fibres were also arranged in a similar manner as in WT cells (21% aligned and 74% radial fibres), but the number of proteoglycan granules present in the extracellular matrix was clearly reduced (Figure 4A). In the *hi307* extracellular matrix, the collagen fibres were present (Figure 4A) but, despite relatively normal stacking of chondrocytes (Figure 3A), only 8% of fibrils were aligned and 59% were radial, while 33% lacked a distinct fibre orientation. Although a mutation in β*3gat3* should block the biosynthesis of most GAGs (Table 1), many electron-dense particles (similar to those in WT proteoglycan granules) were observed in the *hi307* mutant (Figure 4A). In the *hi954* mutant, the extracellular matrix was drastically reduced and was limited to a very thin layer between chondrocytes and a slightly thicker layer at the edge of each cartilage element (Figure 4A).

In comparison to other mutants and WT fish, the extracellular matrix from *hi954* appeared richer in electron-dense material and had numerous focal condensations (Figure 5B). Occasionally, short and thick bundles of fibrous material were observed, especially at

the periphery of cartilage elements, but they were not composed of Collagen II, as indicated by the lack of immunostaining [15]. The collagen network was also disrupted in the pic mutant. Normal collagen fibres were occasionally present, whereas short and thick filaments arranged into bundles were found scattered throughout the extracellular matrix in 93% of gaps between *pic* chondrocytes (Figure 4A). The presence of proteoglycan granules in *pic* mutants was common, and they were found unbound as well as associated with collagen fibrils.

Cell membranes and junctions

Cell membranes surrounding WT chondrocytes had many short protrusions that were in contact with the collagen network (Figure 5A). Evagination of the membrane was especially pronounced between chondrocytes that were not in line with the longitudinal axis but were most likely still moving into the final position (intercalating/stacking). A WT-like appearance of the cell membranes was observed in *dak*, *kny* and *hi307* mutants (Figure 5A). Cell membranes from the *pic* mutant were considerably undulated and also had pronounced protrusions (Figure 5A). In contrast, cell membranes from the *hi954* mutant chondrocytes were smooth and free from any protrusions (Figure 5).

Cell junctions were not commonly observed in chondrocytes from WT, *dak*, *pic*, *kny* and *hi307* mutants (data not shown). This is probably because, similarly to the development of mammalian cartilage, soon after cell division, zebrafish chondrocytes become separated from each other by a layer of extracellular matrix. Interestingly, in the *hi954* mutant, minimal extracellular matrix secretion coincided with impaired cell separation. Cell junctions were maintained and often spanned relatively long fragments of cell membranes (Figure 5B). In consequence, the cells failed to separate, creating clusters of interconnected cells.

Intracellular ultrastructure of chondrocytes

The nuclei of the chondrocytes were well preserved in all fish strains. WT nuclei had regular shapes. Similar appearances of the nuclei were also observed in *dak*, *kny* and *hi307* mutants (Figure 5A). The shape of *hi954* nuclei reflected the shape of the cell, as less regular but still relatively normal. The *pic* mutant was the only one to show nuclei with irregular shapes (Figure 5A). Moreover, pic chondrocytes had mixed populations of normal- and dark-stained cells, with the latter resembling paraptotic T9-C2 cells [16]. An occasional margination of chromatin was observed in the *hi954* mutant only (data not shown). The mitochondria, ER and Golgi apparatus were confirmed in WT and all mutants but, as they showed signs of osmotic stress, they were not subjected to further analysis. This apparently damaged appearance was restricted to chondrocytes only and was observed regardless of the type of fixative. Despite the poor preservation of Golgi, in their close proximity, well-preserved centrioles/basal bodies of primary cilia having typical (9 + 0) microtubule arrangements

were found in WT and all mutant lines (data not shown).

Cytoplasmic inclusions

The presence of glycogen deposits in the cytoplasm has been reported in osteochondroma [17]. We expected to see similar deposits, at least in the *dak* mutant. To our surprise, the transmission electron microscopy images revealed that the cartilage cytoplasms of all six fish lines were devoid of an electron-dense material resembling glycogen. Furthermore, PAS staining for glycogen was negative in the zebrafish cytoplasm (data not shown). Black speckles looking like lipid droplets were found in all fish but only in a small population of chondrocytes, of which all had dark and irregular nuclei resembling cells undergoing cell death (data not shown). Large empty-looking areas devoid of electron-dense material were found in the cytoplasms of all analysed fish (Figure 5A). The content and function of those vacuoles remain unknown.

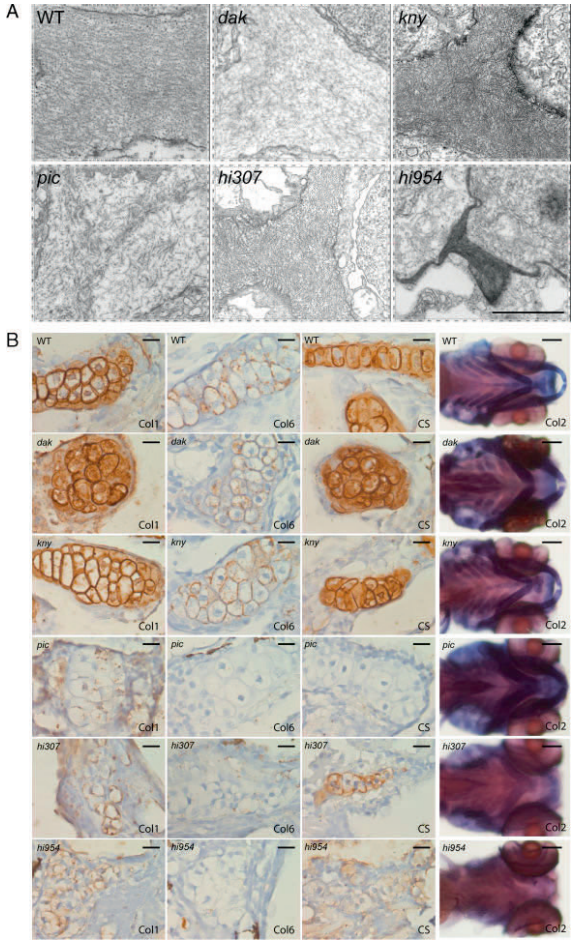

Figure 4. The organization of the extracellular matrix, unequally affected in different mutants. knypek (kny/gpc4) and dackel (dak/ext2) have WT-like collagen networks, whereas pincher (pic/slc35b2) shows a very severe disorganization of the collagen network (bundles of short fibres) (A). Only the remains of the extracellular matrix and no collagen fibres are observed in the hi954 (uxs1) mutant. Surprisingly, hi307 (β3gat3) shows only slight abnormalities in the length and orientation of the collagen network. Electron-dense particles of proteoglycans are observed in all mutants; however, their number is clearly reduced in the dak and hi954 mutants and is surprisingly unaffected in the hi307 mutant. Collagen I, Collagen II, Collagen VI and CS were immunodetected in WT and homozygote mutants at 5 dpf (B). Scale bar = 1 µm (A, B; Col1, Col2, CS) and 10 µm (B; Col2)

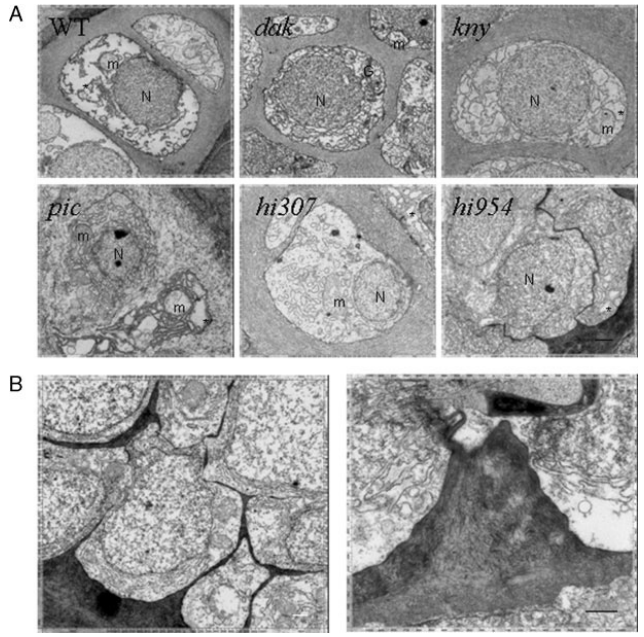

Figure 5. The ultrastructure of chondrocytes in the dackel (dak/ext2), knypek (kny/gpc4), pinscher (pic/slc35b2), hi307 (β3gat3) and hi954 (uxs1) mutants. No apparent ultrastructural changes can be observed in dak, kny and hi307. pic has two types of cells (dark and pale), severe membrane undulation and frequent cell junctions; hi954 has smooth membranes that often fail to separate. Electron micrographs show the chondrocyte ultrastructure (A). Abnormal cell junctions and extracellular matrix are seen in the hi954 homozygote mutant (B). N, nucleus; G, Golgi apparatus; m, mitochondria; *, areas devoid of electron-dense material. Scale bar = 1 μm.

Discussion

The zebrafish skeleton is composed of cartilage and bones, for which the organization and development is underlined by molecular mechanisms similar to those in mammals [18]. Here, we characterized the phenotypic changes caused by proteoglycan deficiencies in zebrafish, with the goal of shedding light on the function of proteoglycans in human skeletogenesis as well as on skeletal disorders for which mutations are still unknown [19].

A summary of the defects found in each mutant is presented in Table 2. In short, *dak* (which is mutated in the *ext2* gene) displays severe cartilage malformation and bone impairment, mild ultrastructural defects and a mild reduction of the body length; *kny* (which is mutated in *gpc4*) has very mild cartilage and bone phenotypes and no obvious ultrastructural defects, but it displays severe dwarfism; *pic*, which is mutated in *slc35b2* (*papst1*), has severe cartilage and bone defects, shows pronounced ultrastructural abnormalities (abnormal collagen filaments, enhanced cell death, frequent cell junctions), displays dwarfism and does not stain with basic dyes; *hi307* (which is mutated in β*3gat3*) has a very mild cartilage and bone phenotype, shows ultrastructural abnormalities restricted to slightly abnormal collagen fibrils, displays dwarfism and does not stain with basic dyes; lastly, *hi954* (which is mutated in *uxs1*) has a severe cartilage and bone phenotype, shows severe ultrastructural defects (reduced extracellular matrix, lack of Collagen II, fused cells, abnormal fibrils), displays dwarfism and does not stain with alcian or toluidine blue.

Table 2. Overview of the defects found in each analysed mutant and information on the human correlates.

name affected gene	WT	*dak ext2*	*pic slc35b2*	*kny gpc4*	*hi307 b3gat3*	*hi954 uxs1*
function		Glycosyltransferase involved in the elongation of the heparan sulphate, chain, forms complexes with EXT1	Adenosine 3′-phospho 5′-phosphosulphate (PAPS) transporter, required for transport of sulphate donors into Golgi	Protein core of Glypican 4 membrane-associated proteoglycan that plays a role in the control of cell division and growth regulation	Glucuronyltransferase involved in the final step of the biosynthesis of the linkage region of proteoglycans	UDP-glucuronate decarboxylase needed for the formation of UDP-xylose and latter initiation of GAG biosynthesis on the protein core of proteoglycans
zebrafish chromosome		7	20	14	7	13, 9
human homologue		*EXT2*	*SLC35B2*	*GPC4*	*β3GAT3*	*UXS1*
human chromosome		11 (p12-p11)	6 (p12.1-p11.2)	X (q26.1)	11 (q12.3)	2 (q12.2)
human disorder		Solitary and multiple osteochondromas		One case with deletion of GPC4 in addition to GPC3 in Simpson–Golabi–Behmel syndrome		
chondrocyte stacking	Normal	Severely impaired	Severely impaired	Partially impaired	Partially impaired	Impaired
ossification	Normal	Lost in some dermal and in all cartilage bones	Lost in most bones	Normal	Delay in cartilage bones	Delay in cartilage bones
perichondrium	Normal	Normal	Thicker	Normal	Normal	Missing
Alcian blue	Blue stain	Blue stain	Unstained	Blue stain	Unstained	Unstained
Toluidin blue	Purple stain	Purple stain	Unstained	Purple stain	Unstained	Unstained
collagen I	+	+	±	+	±	±
collagen II	+	+	+	+	±	−
collagen VI	+	+	−	+	−	−
CSPG	+	+	−	+	±	−
ECM fibers	Normal	Normal	Bundles	Normal	Less frequent	Absent
ECM granules	Normal	Reduced	Reduced	Normal	Normal	Absent
nucleus	Normal	Normal	Dark and pale cells	Normal	Normal	Normal
undulation of cell membranes	Mild	Mild	Severe	Mild	Mild	Absent
cell death	Occasional	Occasional	Common	Occasional	Occasional	Occasional
cell fusion	Absent	Absent	Absent	Absent	Absent	Partial
cell junctions	Seldom present	Seldom present	Often present	Seldom present	Seldomly present	Often present
body length	Normal	Slightly shorter	Dwarfism	Severe dwarfism	Dwarfism	Dwarfism
craniofacial skeleton	Normal	Severely deformed	Deformed	Deformed	Deformed	Deformed
references		9, 13, 26	9, 13	11, 32	10, 14	10, 14, 15

Staining intensity: +, strong; ± , weak; −, absent. More information on zebrafish mutants can be found at ZFIN, the zebrafish model organism database (http://zfin.org/cgi-bin/webdriver?MIval = aa-fishselect.apg).

The similarities in the cartilage phenotype and its severity in *dak* (*ext2*; lacking HS), *pic* (*slc35b2*; lacking sulphation of various molecules, e.g., HS, CS, DS and KS) and *hi954* (*uxs1*; lacking Notch and most proteoglycans) strengthen the importance of HS in cartilage morphology and ultrastructure [this report and 13, 15]. We anticipated that the lack of β*3gat3* in the *hi307* mutant would result in a total inhibition of the biosynthesis of HS, CS and DS and would consequently cause a severe phenotype but, to our surprise, it showed a relatively normal cartilage morphology. The presence of a mutation was confirmed by PCR in all phenotyped *hi307* homozygote mutants (data not shown). However, the presence of other copies or splice variants of β*3gat3* or the involvement of other genes having rescuing effects on the cartilage morphology cannot be excluded. Two other possibilities should be mentioned. First of all, GAGs have been described as the active part of proteoglycans, although it is possible that the protein cores might also be biologically active. Secondly, even if the mutation in β*3gat3* totally inhibited HS, CS and DC, proteoglycans consisting of a protein core and a very short linker (a chain of up to four sugars) could be synthesized; indeed, we found electron-dense particles in the *hi307* mutant. It is possible that these incomplete proteoglycans are sufficient to maintain the cartilage morphology, although a more detailed analysis of the GAGs in *hi307* might yield other explanations of this unexpectedly mild phenotype.

There is no doubt that proteoglycans are important for cartilage development; however, questions have been raised as to whether proteoglycans are necessary, sufficient or non-essential for the induction of bone calcification [20]. Our findings imply that GAGs are not needed for intramembranous ossification (*hi307* and *hi954*); however, reduced sulphation (*pic*) had a strong negative impact on both intramembranous and endochondral bone formation. At 5 dpf, zebrafish are just starting the ossification of cartilage bones, so conclusions about the influence of proteoglycans on endochondral ossification are premature. Carey [21] suggested that proteoglycans are not needed for cell viability or proliferation but that they are necessary for stable extracellular matrix assembly and extracellular matrix–cell interaction. Our data support this hypothesis, as severe defects in cartilage organization, including ultrastructural changes in the extracellular matrix, were observed in zebrafish with mutations in *uxs1* (*hi954*), β*3gat3* (*hi307*) and *slc35b2* (*pic*).

Transmission electron microscopy fixation is known to have an impact on the morphology of cartilage. Chemical fixation of mammal cartilage in the absence of a cationic dye results in chondrocytes having a shrunken appearance and seeming to be surrounded by haloes. This is because many components of the surrounding matrix are lost by aqueous extraction, plasma membrane–extracellular matrix connections are lost, and a pericellular lacuna free of fibrillar collagen and proteoglycans, referred to as a rim, is formed. Similar fixation methods seem to work well for the extracellular matrix in zebrafish craniofacial cartilage, but internal structures such as the mitochondria, ER and Golgi apparatus show compromised preservation. However, as different fixatives resulted in similar chondrocyte

morphologies, it might be possible that this chondrocyte appearance is actually not an artefact but reflects changes occurring with time. Even if fine ultrastructural details might be affected and if topological relationships are sometimes difficult to interpret, potential fixation artefacts are expected to be identical for all the embryos, allowing conclusions to be drawn on the differences between WT and mutant cartilage. It is not clear why similar glycogen deposits were not observed in zebrafish cytoplasm. However, as glycogen deposition seems to increase upon cartilage differentiation [22], it is possible that zebrafish chondrocytes at 5 dpf behaved like resting chondrocytes and had not yet started to accumulate glycogen.

To date, several human disorders have been found to share phenotypical similarities with corresponding zebrafish models [13, 23–25]. The dak zebrafish mutant used in this study has a human correlate: solitary and multiple osteochondromas caused by mutation in the *EXT1* or *EXT2* genes [13, 26–28]. A deletion of *GLYPICAN 4* was described in one patient with Simpson–Golabi–Behmel syndrome [29]. However, this deletion coincided with a mutation in the neighbouring gene, *GLYPICAN 3*, which on its own is a sufficient causative of Simpson–Golabi–Behmel syndrome. It is rather unlikely that *GLYPICAN 4* is involved in the patient overgrowth phenotype, but it could contribute to the craniofacial phenotype and hydrocephalus [30, 31]. These conclusions are supported by the *kny* mutant zebrafish, where a mutation of the fish *glypican 4* results in a short body length and craniofacial phenotype at the larvae stage; additionally, when Gpc4 function is rescued by an injection of WT-mRNA, some embryos survive and grow to be adults with normal overall body lengths [32]. However, those rescued mutants have smaller heads with short and thick jaw bones, forming domed skulls. Interestingly, even though they often miss some facial bones, their jaws remain functional [32]. Hence, it is quite likely that a mutation in *GLYPICAN 4* only might cause a condition that sometime coincides with Simpson–Golabi–Behmel syndrome, influencing its phenotypic variability. Judging by the severity of the cartilage phenotypes found in homozygous fish mutants, putative mutations in human *GPC4* or β*3GAT3* should not cause skeletal problems in early life, whereas mutations in *SLC35b2* or *UXS1* might be involved in the more symptomatic changes already seen prenatally or in toddlers. At present, *pic*, *hi307* and *hi954* zebrafish models cannot be linked with any human disorders, but mutations in related genes are known to cause several skeletal dysplasias. For example, a mutation in *GLYPICAN 6* causes recessive omodysplasia [5], a loss of function of NST (which is encoded by *SLC35D1*) causes Schneckenbecken dysplasia [33], and mutations in *DTDST* (*SLC26A2* sulphate transporter) result in achondrogenesis type 1B, atelosteogenesis type 2 and diastrophic dysplasia [34]. There are many more dysplasias for which the causative mutations are not known [19]. Some of them have been mapped and, interestingly, a few match the locations of the genes we modelled in zebrafish. For instance, split-hand/foot malformation 2 was linked to Xq26, where *GLYPICAN 4* has its locus [35]. However, one has to keep in mind that Xq26 contains other genes besides *GPC4*, including *SLC25A6*, *SLC26A5*

and *HS6ST2*, which might be involved in disorders caused by proteoglycan deficiencies. For those diseases that are not mapped, phenotype matching might be useful. In Table 2, we present a summary of the defects found in each mutant, which can be used as a guideline to help link human diseases with the genes. With this work, we also aim to promote zebrafish as a model for studying human skeletal development and associated pathologies.

Acknowledgements

This work was supported by the European Network of Excellence (EuroBoNeT: http://www.eurobonet.eu), Grant No. 018814 (LSHC-CT-2006-018814), to PCWH. RBGR and MCA acknowledge financial support from NWO under Project No. 016.072.321. The hybridoma collagen II (II-II6B3) antibody developed by T. Linsenmayer was obtained from the Developmental Studies Hybridoma Bank.

Statement of author contributions

MIW and PCWH were involved in the study design; MIW, CMA, FAP and RBGR collected the data; MIW, CMA, CEdeA and RBGR analysed the data; MIW, CEdeA, AJK and PCWH interpreted the data; MIW, CMA and PCWH did literature searches; MIW, CMA, CEdeA, FAP and RBGR generated figures. All authors were involved in writing the paper and had final approval of the submitted and published versions.

References

1. Willems SM, Wiweger M, Frans Graadt van Roggen J, et al. Running GAGs: myxoid matrix revisited. What's in it for the pathologist? Virchow Arch 2009; 456: 181–192.
2. Bovée JVMG, Hogendoorn PCW. Multiple osteochondromas. In World Health Organization Classification of Tumours. Pathology and Genetics of Tumours of Soft Tissue and Bone, FletcherCDM, UnniKK, MertensF (eds). IARC Press: Lyon, 2002; 360–362.
3. Arikawa-Hirasawa E, Wilcox WR, Le AH, et al. Dyssegmental dysplasia, Silverman–Handmaker type, is caused by functional null mutations of the perlecan gene. Nat Genet 2001; 27: 431–434.
4. Pilia G, Hughes-Benzie RM, MacKenzie A, et al. Mutations in GPC3, a glypican gene, cause the Simpson–Golabi–Behmel overgrowth syndrome. Nat Genet 1996; 12: 241–247.
5. Campos-Xavier AB, Martinet D, Bateman J, et al. Mutations in the heparan-sulfate proteoglycan glypican 6 (GPC6) impair endochondral ossification and cause recessive omodysplasia. Am J Hum Genet 2009; 84: 760–770.
6. Thiele H, Sakano M, Kitagawa H, et al. Loss of chondroitin 6-O-sulfotransferase-1 function results in severe human chondrodysplasia with progressive spinal involvement. Proc Natl Acad Sci USA 2004; 101: 10155–10160.

7. Hermanns P, Unger S, Rossi A, et al. Congenital joint dislocations caused by carbohydrate sulfotransferase 3 deficiency in recessive Larsen syndrome and humero-spinal dysostosis. Am J Hum Genet 2008; 82: 1368–1374.
8. Schilling TF, Kimmel CB. Musculoskeletal patterning in the pharyngeal segments of the zebrafish embryo. Development 1997; 124: 2945–2960.
9. Schilling TF, Piotrowski T, Grandel H, et al. Jaw and branchial arch mutants in zebrafish I: branchial arches. Development 1996; 123: 329–344.
10. Golling G, Amsterdam A, Sun Z, et al. Insertional mutagenesis in zebrafish rapidly identifies genes essential for early vertebrate development. Nat Genet 2002; 31: 135–140.
11. Solnica-Krezel L, Stemple DL, Mountcastle-Shah E, et al. Mutations affecting cell fates and cellular rearrangements during gastrulation in zebrafish. Development 1996; 123: 67–80.
12. Kimmel CB, Ballard WW, Kimmel SR, et al. Stages of embryonic development of the zebrafish. Dev Dyn 1995; 203: 253–310.
13. Clément A, Wiweger M, von der Hardt S, et al. Regulation of zebrafish skeletogenesis by ext2/dackel and papst1/pinscher. PLoS Genet 2008; 4: e1000136.
14. Nissen RM, Amsterdam A, Hopkins N. A zebrafish screen for craniofacial mutants identifies wdr68 as a highly conserved gene required for endothelin-1 expression. BMC Dev Biol 2006; 6: 28.
15. Eames BF, Singer A, Smith GA, et al. UDP xylose synthase 1 is required for morphogenesis and histogenesis of the craniofacial skeleton. Dev Biol 2010; 341: 400–415.
16. Hoa N, Myers MP, Douglass TG, et al. Molecular mechanisms of paraptosis induction: implications for a non-genetically modified tumor vaccine. PLoS ONE 2009; 4: e4631.
17. de Andrea CE, Wiweger M, Prins F, et al. Primary cilia organization reflects polarity in the growth plate and implies loss of polarity and mosaicism in osteochondroma. Lab Invest 2010; 90: 1091–1101.
18. Yelick PC, Schilling TF. Molecular dissection of craniofacial development using zebrafish. Crit Rev Oral Biol Med 2002; 13: 308–322.
19. Superti-Furga A, Unger S. Nosology and classification of genetic skeletal disorders: 2006 revision. Am J Med Genet A 2007; 143: 1–18.
20. Hunter GK. Role of proteoglycan in the provisional calcification of cartilage. A review and reinterpretation. Clin Orthop Relat Res 1991; 262: 256–280.
21. Carey DJ. Biological functions of proteoglycans: use of specific inhibitors of proteoglycan synthesis. Mol Cell Biochem 1991; 104: 21–28.

22. Mitchell NS, Shepard NL. Electron microscopic evaluation of the occurrence of matrix vesicles in cartilage. Anat Rec 1990; 227: 397–404.
23. Bassett DI, Currie PD. The zebrafish as a model for muscular dystrophy and congenital myopathy. Hum Mol Genet 2003; 12(2):(spec No): R265–270.
24. Telfer WR, Busta AS, Bonnemann CG, et al. Zebrafish models of collagen VI-related myopathies. Hum Mol Genet 2010; 19: 2433–2444.
25. Venkatasubramani N, Mayer AN. A zebrafish model for the Shwachman–Diamond syndrome (SDS). Pediatr Res 2008; 63: 348–352.
26. Lee J-S, von der HS, Rusch MA, et al. Axon sorting in the optic tract requires HSPG synthesis by ext2 (dackel) and extl3 (boxer). Neuron 2004; 44: 947–960.
27. Hameetman L, Szuhai K, Yavas A, et al. The Role of EXT1 in non-hereditary osteochondroma:identification of homozygous deletions. J Natl Cancer Inst 2007; 99: 396–406.
28. Bovée JVMG. Multiple osteochondromas. Orphanet J Rare Dis 2008; 3: 3.
29. Veugelers M, Vermeesch J, Watanabe K, et al. GPC4, the gene for human K-glypican, flanks GPC3 on Xq26: deletion of the GPC3–GPC4 gene cluster in one family with Simpson–Golabi–Behmel syndrome. Genomics 1998; 53: 1–11.
30. Veugelers M, Cat BD, Muyldermans SY, et al. Mutational analysis of the GPC3/GPC4 glypican gene cluster on Xq26 in patients with Simpson–Golabi–Behmel syndrome: identification of loss-of-function mutations in the GPC3 gene. Hum Mol Genet 2000; 9: 1321–1328.
31. Lindsay S, Ireland M, O'Brien O, et al. Large scale deletions in the GPC3 gene may account for a minority of cases of Simpson–Golabi–Behmel syndrome. J Med Genet 1997; 34: 480–483.
32. LeClair EE, Mui SR, Huang A, et al. Craniofacial skeletal defects of adult zebrafish gypican 4 (knypek) mutants. Dev Dyn 2009; 238: 2550–2563.
33. Hiraoka S, Furuichi T, Nishimura G, et al. Nucleotide–sugar transporter SLC35D1 is critical to chondroitin sulfate synthesis in cartilage and skeletal development in mouse and human. Nat Med 2007; 13: 1363–1367.
34. Rossi A, Superti-Furga A. Mutations in the diastrophic dysplasia sulfate transporter (DTDST) gene (SLC26A2): 22 novel mutations, mutation review, associated skeletal phenotypes, and diagnostic relevance. Hum Mutat 2001; 17: 159–171.
35. Faiyaz-Ul-Haque M, Zaidi SHE, King LM, et al. Fine mapping of the X-linked split-hand/split-foot malformation (SHFM2) locus to a 5.1-Mb region on Xq26.3 and analysis of candidate genes. Clin Genet 2005; 67: 93–97.

Supporting Information

Supporting Information: Table S1. Summary of bone ossification in WT and homozygous mutant fish at 5 days post-fertilization.

name	AB	*dak*	*pic*	*kny*	*hi307*	*hi954*
affected gene	WT	*ext2*	*papst1*	*gpc4*	*b3gat3*	*uxs1*
Maxilla	nd	nd	nd	nd	nd	nd
Dentary	nd	nd	nd	nd	nd	nd
Entopterygoid	nd	nd	nd	nd	+	nd
Parasphenoid	+	nd	+/-	+	+	+
Branchiostegal rays	+	nd	nd	+	+	+
Opercle	+	+	+	+	+	+
Cleithrum	+	+	+	+	+	+
Retroarticular	nd	nd	nd	nd	nd	nd
Quadrate	nd	nd	nd	nd	nd	nd
Ceratohyal	nd	nd	nd	nd	nd	nd
Hyomandibula	nd	nd	nd	nd	+	nd
5th ceratobranchial	+	+	nd	+	+	+
Pharyngeal teeth	+	+	+/-	+	+	+
Notochord	+	+/-	nd	+	+/-	+/-

+, calcification detected by staining with alizarin red; +/-, reduced ossification in comparison to WT and siblings; nd, staining not detected; light grey, dermal bones; medium grey, cartilage bones; dark grey, other bones.

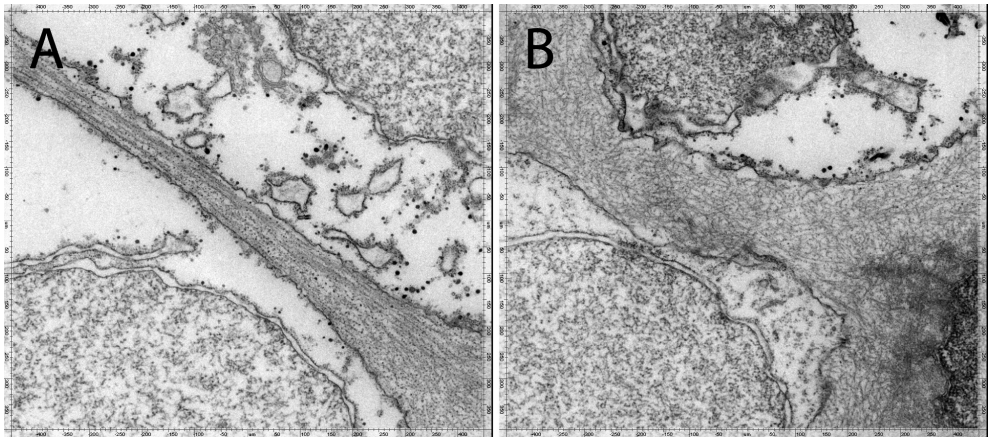

Supporting Information: Figure S1. Examples of the fibrillar organization found in the extracellular matrix of WT zebrafish at 5 days post-fertilization. Between the well-stacked chondrocytes, the fibres are mostly orientated parallel to the longitudinal axis of the cartilage elements (aligned fibres) (A), whereas presumptively intercalating chondrocytes are surrounded by a radially running collagen network (radial fibres) (B).